

A neural network super-resolution approach for the reconstruction of coastal sea states

Jannik Fernando Kuehn¹, Stéphane Marc Abadie¹, and Volker Roeber¹

¹Université de Pau et des Pays de l'Adour

November 21, 2022

Abstract

In this paper, a neural-network-based super-resolution technique is applied to the reconstruction of significant wave height and other sea state variables calculated over coarse meshes by a spectral wave model. The potential of the technique is demonstrated in a case study and the efficiency of the training process as well as the requirements with respect to data quality are analyzed. In this particular example, reasonable accuracy is achieved using only one year of training data with the help of traditional Machine Learning methods like Transfer Learning and Data Augmentation. The presented method leads to up to 50-times lower computation time in comparison to an equivalent traditional direct modeling approach at fine resolution. Overall, incorporation of the presented method into major wave forecasting systems has the potential to allow for the creation of “zoomed-in” areas of interest without the requirement for supplementary calculations at higher resolution.

1 **A neural network super-resolution approach for the**
2 **reconstruction of coastal sea states**

3 **J. Kuehn¹, S. Abadie¹, V. Roeber¹**

4 ¹Université de Pau et des Pays de l'Adour, E2S-UPPA, chair HPC-Waves, SIAME, Anglet, France

5 **Key Points:**

- 6 • Deep learning super-resolution methods can be used to reconstruct coastal sea states.
7 • The method can substitute high-resolution results from low-resolution computa-
8 tions.
9 • Super-resolution can provide local high-resolution wave forecasts without addi-
10 tional computations in operational models.

Corresponding author: Jannik Kuehn, jannik.kuehn@outlook.de

11 Abstract

12 In this paper, a neural-network-based super-resolution technique is applied to the
13 reconstruction of significant wave height and other sea state variables calculated over coarse
14 meshes by a spectral wave model. The potential of the technique is demonstrated in a
15 case study and the efficiency of the training process as well as the requirements with re-
16 spect to data quality are analyzed. In this particular example, reasonable accuracy is
17 achieved using only one year of training data with the help of traditional Machine Learn-
18 ing methods like Transfer Learning and Data Augmentation. The presented method leads
19 to up to 50-times lower computation time in comparison to an equivalent traditional di-
20 rect modeling approach at fine resolution. Overall, incorporation of the presented method
21 into major wave forecasting systems has the potential to allow for the creation of “zoomed-
22 in” areas of interest without the requirement for supplementary calculations at higher
23 resolution.

24 Plain Language Summary

25 Accurate wave height forecasts on a daily basis are essential for many coastal com-
26 munities worldwide. Though multiple operational wave models provide access to global
27 wave forecasts, local high-resolution output is often not available. In this paper, we pro-
28 pose an approach based on neural networks to convert low-resolution computations into
29 higher resolution. In our case study, this method is reasonably accurate, it enhances the
30 resolution up to 16 times, and can be more than 50 times faster than what is required
31 for the actual high-resolution calculation. After a one-time training process of the neu-
32 ral network, it has the potential to be incorporated into major forecasting systems, al-
33 lowing to “zoom” into specific regions of interest in real-time.

34 1 Introduction

35 Many coastal communities rely on daily wave height forecasts for the purpose of
36 safety and hazard mitigation. Over the last decades, improvements in numerical meth-
37 ods have lead to more accurate predictions of sea states, which had a considerable in-
38 fluence on marine transport, fisheries, and ocean engineering. Global efforts of produc-
39 ing ocean observation networks paired with national ocean services (e.g., the National
40 Oceanic and Atmospheric Administration), national and international buoy networks (e.g.,
41 the CANDHIS network in France - <https://candhis.cerema.fr>), and global ocean wave
42 models like SWAN (Booij et al., 1999) and WAVEWATCH III (Tolman, 2009) provide
43 critical information - often in real-time. However, high-resolution data, particularly in
44 the coastal zone, is often missing due to computational constraints associated with large
45 computational domains in combination with fine meshes. Nevertheless, the need for lo-
46 cal high-resolution data still exists at this scale, since local forecasts for wave-driven pro-
47 cesses are increasingly based on refined computations.

48 The recent rise in interest in Machine Learning and its ongoing integration into nat-
49 ural sciences can be largely attributed to its ability to perform various computational
50 tasks faster and with similar accuracy after an initial training phase has been completed.
51 In this article we present a super-resolution approach to decrease computation time for
52 forecasts of up to 50 times compared to traditional direct modeling of an equivalent do-
53 main at fine resolution. The idea is based on training a neural network that converts low-
54 resolution (LR) results to a higher resolution for a specific study area. The main advan-
55 tage of this approach is that the computation of a low-resolution forecast and the sub-
56 sequent conversion are considerably faster than a direct high-resolution (HR) computa-
57 tion. Furthermore, once trained, this model has the potential to be directly linked to the
58 output of global ocean wave models, thus providing local high-resolution results on the
59 fly without the need for costly direct calculations.

60

61 Super-resolution has been an active field of research in computer vision for almost
 62 a decade. Recently, it also started to be applied to fluid mechanics - especially in the field
 63 of turbulence (Kim et al., 2020; Gao et al., 2021). In ocean sciences, deep-learning-based
 64 super-resolution was already successfully applied to remote sensing data of sea-surface
 65 temperature (Ducournau & Fablet, 2016; Su et al., 2021). Furthermore, treating grid-
 66 ded bathymetric data as digital images, Sonogashira et al. (2020) enhanced the resolu-
 67 tion of coarse bathymetric charts by outperforming naive interpolation. This showcased
 68 that super-resolution might considerably reduce the amount of measurements needed.
 69 Even though previous papers addressed the need for improving local forecasts with neu-
 70 ral networks (Londhe et al., 2016; James et al., 2018), this is the first time, to the best
 71 of our knowledge, that super-resolution techniques are applied to coastal wave model-
 72 ing.

73

74 In the present paper, we propose to apply the Downsampled Skip-Connection Multi-
 75 Scale (DSC/MS) neural network introduced by Fukami et al. (2019) to convert low-resolution
 76 SWAN computations to an up to 16-times higher resolution. In the first part of this pa-
 77 per, the workflow is explained with a focus on data processing and potential data en-
 78 hancement methods. We then present the results from an application of the model to
 79 a study case for the nearshore area at Biarritz (SW France). Lastly, we discuss our re-
 80 sults, the presently existing limitations of this approach, and the potential for future re-
 81 search.

82 2 Materials and Methods

83 As a first step to construct a framework for neural-network-based super-resolution
 84 it is necessary to obtain a training and test data set from a coastal wave model .

85 2.1 SWAN and Data Pre-processing

86 For the creation of a data set with matching LR and HR images, we compute var-
 87 ious quantities including significant wave height H_S , peak wave period T_P and mean wave
 88 direction θ with the third-generation spectral wave model SWAN (Simulating WAVes Nearshore)
 89 (Booij et al., 1999) for a part of the coastal area near Biarritz (Fig. 1).

90 The area of interest is nested inside a coarser grid that is forced by homogeneous
 91 spectral boundary conditions taken from the HOMERE hindcast database (Edwige et
 92 al., 2013), at the location of the Donostia buoy (i.e., around 35km from Biarritz in a wa-
 93 ter depth of about 450 m). The wave data set, which is considered for this work covers
 94 a two-year time period spanning from January 01, 2018 to December 31, 2019. For the
 95 HR nested grid, we chose a grid with 160 x 160 quadratic cells (8 km in x- and y-direction
 96 with $\Delta x = \Delta y = 50$ m), which is of sufficient resolution to capture small variations in
 97 the wave regime, while enabling down-scaling by multiples of two. Consequently, the cor-
 98 responding LR grids are of size 40 x 40, 20 x 20, and 10 x 10.

99 The bathymetry data was obtained from the publicly-available 0.001 ° precision
 100 Digital Terrain Model "MNT bathymétrique de façade Atlantique" provided by the French
 101 Service Hydrographique et Océanographique de la Marine (SHOM) (SHOM, 2015) and
 102 interpolated with Octave (Eaton et al., 2020) to the various grid sizes.

103 With the objective to demonstrate the feasibility of the application of neural-network-
 104 based super-resolution to ocean wave modeling, we use basic, but still realistic settings
 105 for the SWAN computations. In particular, wind forcing, wind growth, and white-capping
 106 are not taken into account. The water level was set constant and equal to the mean wa-

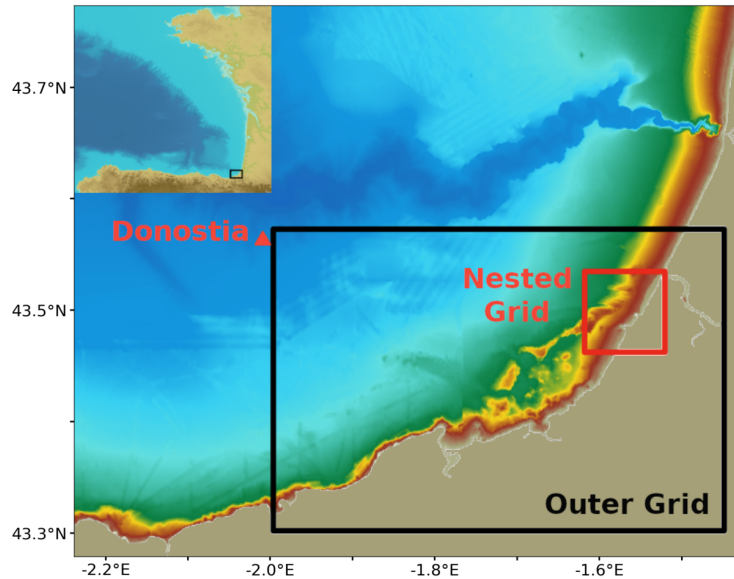


Figure 1. Bathymetry map of the study area and the locations of the outer and the nested grid. (Top left panel : location of the study site on the French Atlantic coast.)

107 ter level 2.25 m. Depth-induced wave breaking was modeled with constant values $\alpha =$
 108 1 and $\gamma = 0.73$ adapted from Battjes and Stive (1985). Bottom friction is based on Madsen
 109 et al. (1988) with a constant coefficient of 0.085.

110 We note that the SWAN model returns NaNs for cells that fall across the coast-
 111 line. Since Neural Networks cannot work with NaNs, they have to be addressed sepa-
 112 rately as discussed in the workflow in section 2.6.

113 2.2 Neural-Network architecture

114 For our neural network architecture, we used the hybrid Downsampled Skip-Connection
 115 Multi-Scale (DSC/MS) model presented in Fukami et al. (2019), given their success in
 116 reconstructing turbulent flows and its easier implementation and much lower training
 117 time as compared to, for example, Generative Adversarial Networks (GAN) (Stengel et
 118 al., 2020). Since quality literature exists on the topic of Deep Learning, Neural Networks,
 119 and more specifically Convolutional Neural Networks (CNN) and their application to im-
 120 age processing, we refer the interested reader to one of the following sources for an in-
 121 troduction to the topic (Guo et al., 2016; Rawat & Wang, 2017; Aloysius & Geetha, 2018).
 122 As for the model employed, it is based on a CNN, but is modified to improve the recon-
 123 struction of both large and small-scale patterns. The modifications include data com-
 124 pression, which makes the network more robust to rotations and translations (Ngiam et
 125 al., 2010) and skipped connections, that reduce difficulties concerning the convergence
 126 of the weights often seen in deep CNNs (He et al., 2016). This is paired with the multi-
 127 scale model by Du et al. (2018), which comprises multiple CNN filters of varying length
 128 to capture a range of scales. For more detailed information, we refer to the original ar-
 129 ticle of the author.

130 2.3 Data Augmentation

131 Improvements of the predictions made by the neural network can be achieved though
 132 an artificial increase of the size of the data set by modifying the labeled data in a real-

133 istic way. This is a common procedure, especially in the area of image recognition (Perez
 134 & Wang, 2017). As an example, a picture of a recognizable object can be mirrored hor-
 135 izontally or the brightness and contrast of the image can be changed, but the object in
 136 the picture would still be recognizable. These artificial modifications help the neural net-
 137 work to generalize better and consequently enhance the results (Shorten & Khoshgof-
 138 taar, 2019).

139 In this study, we perform data augmentation on the significant wave height data
 140 set by adding a random uniformly distributed offset between zero and five meters to each
 141 data instance, to artificially account for wave heights in different regimes. The distribu-
 142 tion parameters are arbitrary but realistic and worked well in our case. Excessively small
 143 or large offsets deteriorate the performance of the data augmentation. It should be noted
 144 that the same offset has to be applied to the input and reference data instances.

145 2.4 Transfer Learning

146 Another commonly used technique when working with neural networks is trans-
 147 fer learning (Pan & Yang, 2010), where some or all of the weights of another already trained
 148 neural network are reused. Indeed, the lower layers of a network tend to learn small-scale
 149 features that might contain useful information for similar tasks.

150 Here, we first create artificial LR input by downsampling the reference HR sam-
 151 ples with average pooling. This operation computes the average over a so-called pool-
 152 ing window that slides with a given stride s over the whole image. In our case the given
 153 HR grid size is 160x160 and the pooling window is 4x4 (resp. 8x8, or 16x16) with a stride
 154 of $s = 4$ (resp. 8, or 16). The output is a LR image with a 40x40 (resp. 20x20, or 10x10)
 155 grid, where each pixel corresponds to an average of a 4x4 (resp. 8x8, or 16x16) part of
 156 the original data instance.

157 We then train the neural network with the average pooled LR images as an input
 158 and the corresponding HR images as the references. Models trained from average pooled
 159 data usually predict well, given that comparatively much of the information is retained
 160 after the downsampling. The weights obtained by training on the averaged pool data are
 161 taken to initialize the weights of the actual neural network, which is trained on the di-
 162 rectly modeled data. This leads to faster convergence and commonly improves the mean
 163 square error (MSE). However, the pre-training on the averaged pool model can take about
 164 as long as training the actual execution of the model, which makes transfer learning com-
 165 putationally expensive. Nonetheless, training is a one-time cost, which is typically com-
 166 pensated by the considerably quicker run time after training.

167 2.5 Bicubic Interpolation

168 It is also possible to upsample the LR image to the reference grid size with bicu-
 169 bic interpolation to further minimize the prediction error. This is a standard technique
 170 in image super-resolution (Dong et al., 2016) and it helped to improve the model results
 171 in our study for certain configurations.

172 2.6 Workflow

173 Our workflow is summarized in Fig. 2. First, the data set is obtained by comput-
 174 ing a coastal wave model over two grids - one with high and the other one with low res-
 175 olution. The data is then split into "snapshots", i.e. into files containing a particular dis-
 176 tribution of a variable (e.g., H_s) across the numerical domain at one time step. In our
 177 case, the sampling interval is one hour in both the high and low resolution data set. As
 178 a next step, it is customary to set aside a certain fraction of the whole data set for test-
 179 ing purposes. Then, the rest of the data is divided into a training and validation set. The

180 former is used by the model to adjust the weights, whereas the latter is for hyper-parameter
 181 tuning and performance assessment of the model after each training epoch. All of the
 182 low-resolution data, including the test data, is upsampled by a simple nearest-neighbor
 183 scheme to enable passing the input to the neural network. This means that if the low-
 184 resolution grid has 4-times less cells, each pixel gets copied 4 times to fill the high-resolution
 185 grid size (Sonogashira et al., 2020). Alternatively, this step is skipped and replaced by
 186 upsampling with a bicubic interpolation method. In all cases, the NaNs resulting from
 187 the coastline of the coastal wave model are replaced by zero, as the neural network han-
 188 dles only numbers. If necessary, the training set is enhanced artificially by performing
 189 data augmentation. Alternatively, or additionally, it is also possible to train a pre-model,
 190 on average-pooled data, of which the weights are then used for transfer learning. After
 191 the optional data treatment the model is trained with ADAM optimization (Kingma &
 192 Ba, 2014) and early stopping (Prechelt, 1998). It is then evaluated with the test set to
 193 obtain a realistic estimation of the performance of the neural network. If required, cer-
 194 tain parameters are adjusted and the model is retrained. Lastly, after a satisfactory re-
 195 sult is reached, the model is trained with all the data available, including the test data
 196 to then deploy the neural network.

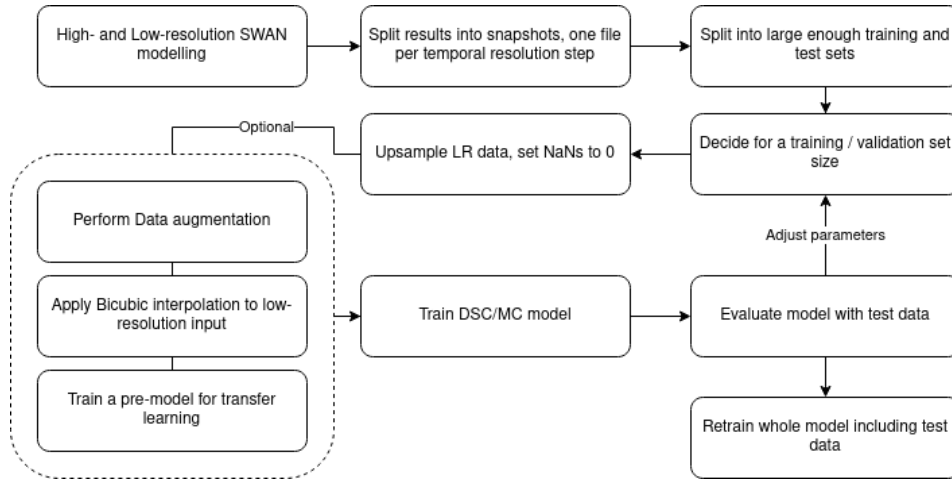


Figure 2. Workflow for training a DSC/MS model from data of a coastal wave model.

197 **2.7 Application**

198 In the present study, we run a pair of high- and low-resolution SWAN computa-
 199 tions for the two year period between January 01, 2018 and December 31, 2019. For each
 200 model, we use the first year for training (80 %) and validation (20 %), and the second
 201 year solely for testing to get a realistic estimation of the performance of the model over
 202 various sea states. We perform data augmentation as described in section 2.3 on 2000
 203 data instances randomly sampled from the training set. Finally, the three models are trained
 204 to convert modeling results of significant wave height to a grid size of 160x160 from one
 205 of 40x40, 20x20, and 10x10, respectively.

206 **3 Results**

207 In Fig. 3 the low-resolution inputs along with the corresponding predictions and
 208 their MSE are shown. For comparison, the high-resolution reference snapshot is displayed
 209 as well. The data instance was chosen as being close to the average wave regime.

210 In the three cases, the high-resolution computations are well approximated by the
 211 reconstructions. The prediction not only correctly captures most of the wave features,
 212 but also reconstructs the original coastline in a sense that the neural network predicts
 213 negligible values (< 0.01) for values on land. Setting values lower than a small thresh-
 214 old to NaN results in a near-perfect reconstruction of the original coastline. This turns
 215 out remarkably well in particular for the third model with an original grid size of 10x10
 216 where the low-resolution input only provides very coarse information regarding wave height
 217 patterns and coastline.

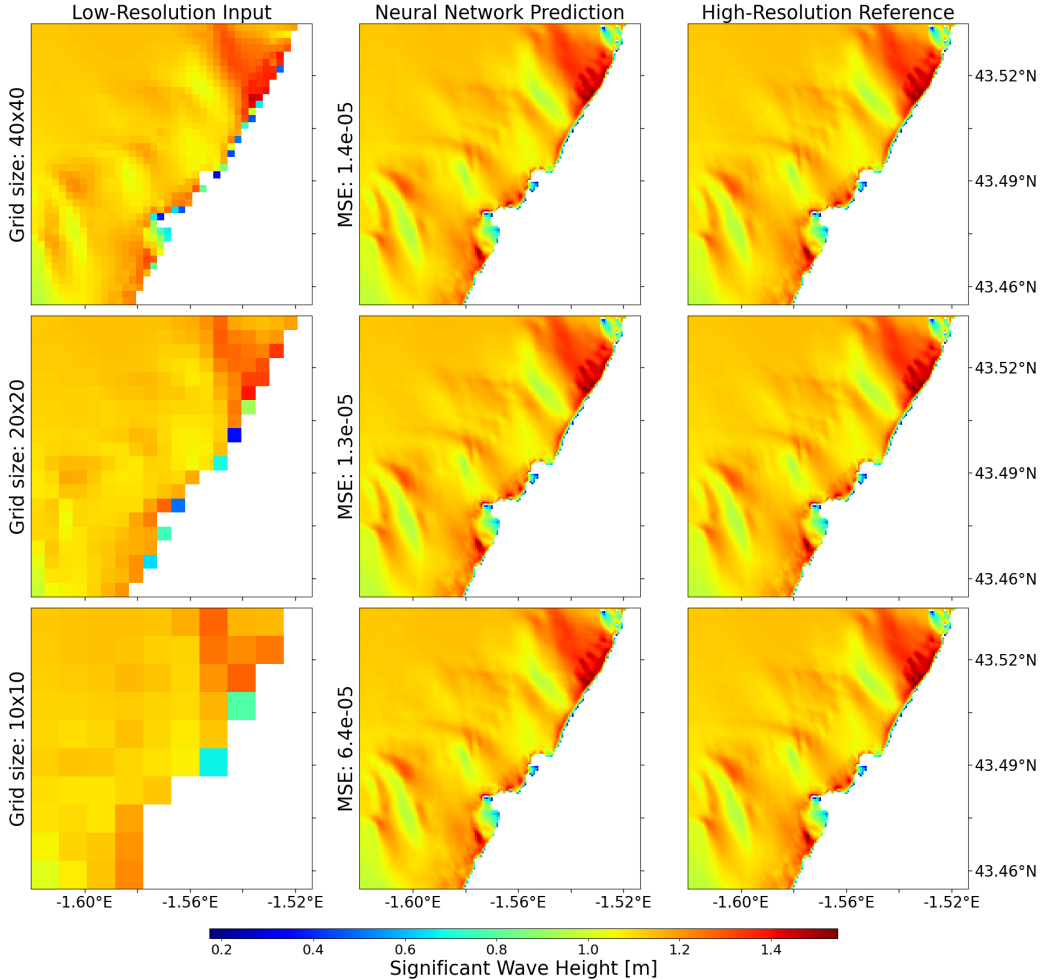


Figure 3. Reconstructions of direct high-resolution computations from different lower resolution calculations. The MSE is shown for the predictions. The data instance is from April 21, 2019 at midnight.

218 In general, the results improved after performing data augmentation or transfer learning.
 219 In certain cases, mostly in models converting 40x40 grid sizes, application of bicu-
 220 bic interpolation also reduced the mean-square error. For other grid sizes, however, pre-
 221 dictions usually deteriorated. Here, only the results without any prior data "enhance-
 222 ment" are shown to demonstrate the feasibility of the method in its simplest form. Var-
 223 ious combinations of the techniques mentioned here, paired with careful hyperparam-
 224 eter tuning, and possible normalization of the data set can significantly improve the pre-
 225 dictions. However, a thorough analysis is beyond the scope of this article.

226 Models trained on the peak wave period or direction performed reasonably well.
 227 However, the overall patterns were not reproduced as sharply and accurately as in the
 228 case of the significant wave height. This might be due to the more heterogeneous nature
 229 of those two variables, as well as larger absolute values. The latter might be mitigated
 230 by prior normalization.

231 For a quantitative overview of the most common reconstruction errors, we compute
 232 the prediction for every data instance in the test data set and subtract it from the cor-
 233 responding reference to obtain the deviation. We then average the LR input, the pre-
 234 diction, the HR references and the errors, which are shown in Fig. 4 for the reconstruc-
 235 tion of a 10x10 grid. The mean errors are commonly the most prominent around the vis-
 236 ible patterns, with a tendency to underestimate large and overestimate small wave heights.
 237 Nonetheless, the average error amounts only to a few centimeters, in consistency with
 238 errors of single data instances. We found that the largest errors occurred in the recon-
 239 struction of very high and very low sea states. This is to be expected, given that those
 240 sea states were the least frequent in our data set and were thus the least represented dur-
 241 ing training. Data augmentation is able to mitigate the errors by generating artificially
 242 more representative sea states, but it is efficient only to a certain extent. This is likely
 243 due to a corresponding structural change of the patterns in the extreme sea states, which
 244 is not taken into account in the data augmentation process. Possible approaches to min-
 245 imize the error further are discussed later.

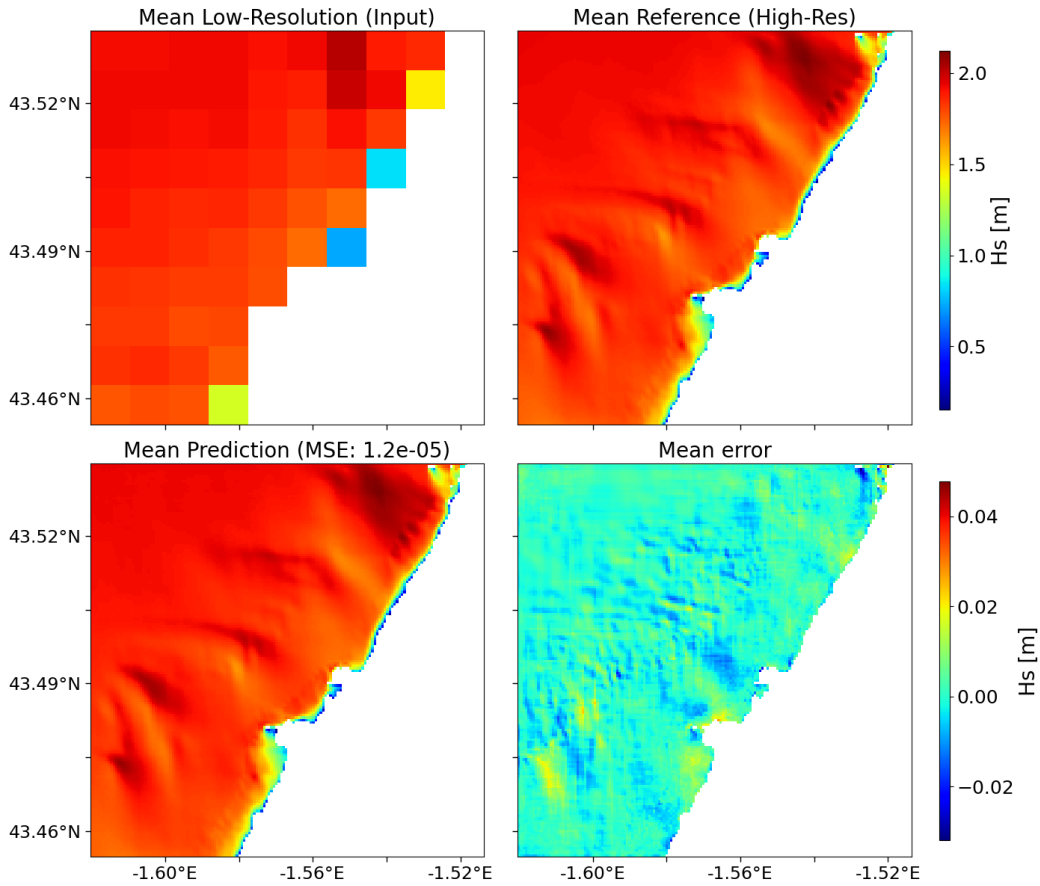


Figure 4. Average reconstruction error over the study area for a 16-times increase in resolution. The mean was taken over the whole test data set.

246 3.1 Comparison of Computation Time

247 To outline the gains in computation time by this approach, we listed the time needed
 248 at all the steps of the method. The SWAN computations were run with 12 parallel threads
 249 on an Inter Core i7-9750H processor with 6 cores and 12 threads. For the pre-processing,
 250 we used the same processor without parallel threading and for training and prediction
 251 of the neural network, a Nvidia GeForce RTX 2070 Max-Q was used.

252

253 As a first step, the outer grid of the SWAN model was computed over the time range
 254 of 2 years, which took around 7.5 h. Similarly, computing the same time range in the nested,
 255 high-resolution 160x160 grid took also 7.5 h. Calculation of the same nested grid in lower
 256 resolutions (40x40, 20x20, 10x10) required only 35 min, 14 min, and 8 min, respectively.

257 Training times of the neural network can change significantly (on the order of 10s
 258 of minutes) for the same model, if the algorithm gets stuck in a local minimum. Usual-
 259 ly pre-processing and training took 2 h - 4 h, but more specifically for our models, the
 260 time required were 2.5 h, 2.5 h, and 3.5 h, respectively. One has to note, however, that
 261 this is only a one-time cost, since in theory the model can be re-used for later calcula-
 262 tions. In practice, occasional re-training with additional data would be advisable.

263 The actual prediction by the model is computed very fast, since, once the weights
 264 are determined after training, predictions are simple matrix multiplications. A conver-
 265 sion of 1000 data instances, which corresponds to around 40 days of hourly significant
 266 wave height, required only 1.9 s.

267

268 In summary, converting 2 years of data of 10x10 LR calculations to 160x160 HR,
 269 takes only around 8.5 min, including the time to run the LR SWAN computations, com-
 270 pared to the 7.5 h when modeling the domain directly in high-resolution, which is a more
 271 than 50-fold increase in computation time.

272 4 Summary and discussion

273 The DSC/MS model proposed by Fukami et al. (2019) is able to reconstruct high-
 274 resolution features of various sea state variables given a low-resolution image. Overall,
 275 this approach has the potential to reduce computation time for forecasts considerably.
 276 After a high, but only single computational effort of training the model, predictions can
 277 be obtained 50-times faster, compared to a standard high-resolution SWAN computa-
 278 tion, with good accuracy. Furthermore, the speed and accuracy presented here are prob-
 279 ably lower bound estimates, which can be ameliorated with a more elaborated pre-processing
 280 routine, an improved model architecture and careful training data sampling. Also, ex-
 281 isting hindcast databases could be used to train the model extensively. Additionally, dif-
 282 ferent loss equations and other neural network architectures like GANs, could improve
 283 the results substantially.

284 Instead of data augmentation a large or well-sampled data set could be used, which
 285 covers many possible wave conditions. This would also very likely improve the predic-
 286 tions. Here, we focus on data augmentation to demonstrate that even with relatively small
 287 training sample sizes, a robust prediction can be achieved for various wave conditions.

288 A drawback of our approach is that one model has to be trained for each wave vari-
 289 able, which increases the training time substantially. Nevertheless, it does not affect the
 290 prediction time. Training one model to predict all variables is possible, however, it de-
 291 teriorates the results as commonly reported in literature (Schultz et al., 2021).

Moreover, the trained models are location-specific and, consequently, a model has to be trained for each new location. As discussed in section 2.4, the training time can be reduced with transfer learning. Another recent approach builds on incorporation of physical equations in the training process to produce so-called Physics-Informed Neural Networks (PINN) (Um et al., 2020; Gao et al., 2021). Commonly, this is done by adding particular terms, like the constraint of zero divergence for incompressible fluids in the loss equations (Raissi et al., 2019). This forces the neural network to not only produce more physically plausible results, but also helps it to better generalize. A thorough overview of PINNs can be found in Willard et al. (2020). While this approach appears difficult to implement in a spectral wave model like SWAN, it might be possible for other wave models relying on different governing equations.

Note also, that in comparison to other applications for instance in fluid mechanics, temporal coherence is much easier to achieve in our setting. This is presumably due to the easier structure of our problem. While a reconstruction of turbulent flows varies strongly in space and time, coastal waves do not exhibit the same amount of variation. For example, Xie et al. (2018) developed a sophisticated Generative Adversarial Network to achieve temporal coherence in their super-resolution reconstruction of smoke flow. However, we observed that for our simpler case temporal coherence was already given with the least complex model that we employed. Lastly, we considered only rectangular, uniform grids due to the simplicity of finding and computing high- and low resolution pairs. Given that many studies use more complex grid structures, more research has to be undertaken to generalize this approach to any type of grid.

Despite the current limitations of the super-resolution method applied to coastal wave modeling, it is able to produce high-resolution results and consistently reconstruct the underlying patterns with remarkable accuracy, while being considerably faster than traditional direct computations. Additionally, it has the potential to be more generic and accurate at equal computation time and could be used in the future for locally "zoomed-in" global wave models.

5 Open Research

5.1 Data Availability

For the creation of the low- and high-resolution sea state quantities we used the third-generation spectral wave model SWAN (Booij et al., 1999), version 41.31. It was forced by data from the HOMERE hindcast database (Edwige et al., 2013) at the location of the Donostia buoy covering the time range from January 1st 2018 to December 31st 2019. Bathymetry data from the 0.001° Digital Terrain Model "MNT bathy-métrique de façade Atlantique" provided by the French Service Hydrographique et Océano-graphique de la Marine (SHOM) (SHOM, 2015) and interpolated with Octave version 5.2.0 (Eaton et al., 2020). The Neural Network in this paper is based on the code and the implementation of Fukami et al. (2019). Pre-processing and training was done entirely in Python 3.9.7, using mostly the following libraries: Keras 2.4.3 (Chollet & Others, 2015) with Tensorflow 2.4.1 as a backend (Abadi et al., 2015), Pandas 1.3.4 (Reback et al., 2021), and Numpy 1.19.2 (Harris et al., 2020). For the creation of the figures Matplotlib 3.5 (Hunter, 2007) was used. The SWAN, pre-processing and training scripts are available through GitHub under https://github.com/janfer95/SR_on_SWAN (Kuehn et al., 2022).

Acknowledgments

This research was carried out under the framework of the joint laboratory KOSTARISK, which is part of the E2S UPPA program managed by the French National Research Agency (ANR-16-IDEX-0002) and supported by the French Government's "Investissements d'Avenir" (PIA). The joint laboratory KOSTARISK is co-funded by E2S UPPA, the AZTI Foun-

341 dation and the center Rivages Pro Tech of SUEZ. The authors acknowledge financial sup-
 342 port from E2S UPPA, the Communauté d’Agglomération Pays Basque (CAPB), and the
 343 Communauté Région Nouvelle Aquitaine (CRNA) for the chair HPC-Waves and the Eu-
 344 ropean Union Horizon 2020 project ALPHEUS - DLV-883553. All of the code was writ-
 345 ten in Python. The Neural Network was implemented with the Keras library having Ten-
 346 sorflow as a backend. The code will be accessible through GitHub.

347 References

- 348 Abadi, M., Agarwal, A., Barham, P., Brevdo, E., Chen, Z., Citro, C., . . . Zheng, X.
 349 (2015). *TensorFlow: Large-Scale Machine Learning on Heterogeneous Systems*.
 350 Retrieved from <https://www.tensorflow.org/>
- 351 Aloysius, N., & Geetha, M. (2018). A review on deep convolutional neural net-
 352 works. *Proceedings of the 2017 IEEE International Conference on Communica-*
 353 *tion and Signal Processing, ICCSP 2017, 2018-Janua*, 588–592. doi: 10.1109/
 354 ICCSP.2017.8286426
- 355 Battjes, J. A., & Stive, M. J. F. (1985). Calibration and verification of a dissipation
 356 model for random breaking waves. *Journal of Geophysical Research*, *90*(C5),
 357 9159. doi: 10.1029/JC090iC05p09159
- 358 Booij, N., Ris, R. C., & Holthuijsen, L. H. (1999, apr). A third-generation wave
 359 model for coastal regions: 1. Model description and validation. *Journal of Geo-*
 360 *physical Research: Oceans*, *104*(C4), 7649–7666. Retrieved from [http://doi](http://doi.wiley.com/10.1029/98JC02622)
 361 [.wiley.com/10.1029/98JC02622](http://doi.wiley.com/10.1029/98JC02622) doi: 10.1029/98JC02622
- 362 Chollet, F., & Others. (2015). *Keras*. <https://keras.io>.
- 363 Dong, C., Change, L. C., & Xiaoou, T. (2016). Accelerating the Super-Resolution
 364 Convolutional Neural Network. *European Conference on Computer Vision*,
 365 391–407. doi: https://doi.org/10.1007/978-3-319-46475-6_25
- 366 Du, X., Qu, X., He, Y., & Guo, D. (2018). Single image super-resolution based on
 367 multi-scale competitive convolutional neural network. *Sensors*, *18*(3), 789.
- 368 Ducournau, A., & Fablet, R. (2016, dec). Deep learning for ocean remote sens-
 369 ing: an application of convolutional neural networks for super-resolution on
 370 satellite-derived SST data. In *2016 9th iapr workshop on pattern recogniton in*
 371 *remote sensing (prrs)* (pp. 1–6). IEEE. Retrieved from [http://ieeexplore](http://ieeexplore.ieee.org/document/7867019/)
 372 [.iee.org/document/7867019/](http://ieeexplore.ieee.org/document/7867019/) doi: 10.1109/PRRS.2016.7867019
- 373 Eaton, J. W., Bateman, D., Hauberg, S., & Wehbring, R. (2020). GNU Octave
 374 version 5.2.0 manual: a high-level interactive language for numerical compu-
 375 tations [Computer software manual]. Retrieved from [https://www.gnu.org/](https://www.gnu.org/software/octave/doc/v5.2.0/)
 376 [software/octave/doc/v5.2.0/](https://www.gnu.org/software/octave/doc/v5.2.0/)
- 377 Edwige, B., Christophe, M., Ardhuin, F., Accensi, M., Pineau-Guillou, L., & Lep-
 378 esqueur, J. (2013). *A suitable metocean hindcast database for the design of*
 379 *Marine energy converters* (Vol. 3-4) [Article]. FRANCE. Retrieved from
 380 https://marc.ifremer.fr/en/produits/hindcast_sea_states_homere doi:
 381 <https://doi.org/10.1016/j.ijome.2013.11.010>
- 382 Fukami, K., Fukagata, K., & Taira, K. (2019). Super-resolution reconstruction of
 383 turbulent flows with machine learning. *Journal of Fluid Mechanics*, *870*(M1),
 384 106–120. doi: 10.1017/jfm.2019.238
- 385 Gao, S., Huang, J., Li, Y., Liu, G., Bi, F., & Bai, Z. (2021, jan). A fore-
 386 casting model for wave heights based on a long short-term memory neu-
 387 ral network. *Acta Oceanologica Sinica*, *40*(1), 62–69. Retrieved from
 388 <https://link.springer.com/article/10.1007/s13131-020-1680-3> doi:
 389 [10.1007/s13131-020-1680-3](https://link.springer.com/article/10.1007/s13131-020-1680-3)
- 390 Guo, Y., Liu, Y., Oerlemans, A., Lao, S., Wu, S., & Lew, M. S. (2016). Deep learn-
 391 ing for visual understanding: A review. *Neurocomputing*, *187*, 27–48. doi: 10
 392 [.1016/j.neucom.2015.09.116](https://doi.org/10.1016/j.neucom.2015.09.116)
- 393 Harris, C. R., Millman, K. J., van der Walt, S. J., Gommers, R., Virtanen, P., Cour-

- 394 napeau, D., ... Oliphant, T. E. (2020). Array programming with NumPy.
 395 *Nature*, 585(7825), 357–362. Retrieved from [https://doi.org/10.1038/](https://doi.org/10.1038/s41586-020-2649-2)
 396 [s41586-020-2649-2](https://doi.org/10.1038/s41586-020-2649-2) doi: 10.1038/s41586-020-2649-2
- 397 He, K., Zhang, X., Ren, S., & Sun, J. (2016). Deep residual learning for image
 398 recognition. In *Proceedings of the IEEE conference on computer vision and pat-*
 399 *tern recognition* (pp. 770–778).
- 400 Hunter, J. D. (2007). Matplotlib: A 2D graphics environment. *Computing in Science*
 401 *& Engineering*, 9(3), 90–95. doi: 10.1109/MCSE.2007.55
- 402 James, S. C., Zhang, Y., & O’Donncha, F. (2018, jul). A machine learning frame-
 403 work to forecast wave conditions. *Coastal Engineering*, 137, 1–10. doi: 10
 404 .1016/j.coastaleng.2018.03.004
- 405 Kim, H., Kim, J., Won, S., & Lee, C. (2020). Unsupervised deep learning for super-
 406 resolution reconstruction of turbulence. *Journal of Fluid Mechanics*, 1–34. doi:
 407 10.1017/jfm.2020.1028
- 408 Kingma, D. P., & Ba, J. (2014). Adam: A method for stochastic optimization. *arXiv*
 409 *preprint arXiv:1412.6980*.
- 410 Kuehn, J., Abadie, S., & Roeber, V. (2022). *janfer95/SR_on_SWAN: Initial Release*.
 411 Zenodo. Retrieved from <https://doi.org/10.5281/zenodo.5910948> doi: 10
 412 .5281/zenodo.5910948
- 413 Londhe, S. N., Shah, S., Dixit, P. R., Nair, T. M., Sirisha, P., & Jain, R. (2016).
 414 A Coupled Numerical and Artificial Neural Network Model for Improving Lo-
 415 cation Specific Wave Forecast. *Applied Ocean Research*, 59, 483–491. doi:
 416 10.1016/j.apor.2016.07.004
- 417 Madsen, O. S., Poon, Y.-K., & Graber, H. C. (1988, jan). SPECTRAL WAVE
 418 ATTENUATION BY BOTTOM FRICTION: THEORY. *Coastal Engineering*
 419 *Proceedings*, 1(21), 34. Retrieved from [https://journals.tdl.org/icce/](https://journals.tdl.org/icce/index.php/icce/article/view/4241)
 420 [index.php/icce/article/view/4241](https://journals.tdl.org/icce/index.php/icce/article/view/4241) doi: 10.9753/icce.v21.34
- 421 Ngiam, J., Chen, Z., Chia, D., Koh, P., Le, Q., & Ng, A. (2010). Tiled convolutional
 422 neural networks. *Advances in neural information processing systems*, 23.
- 423 Pan, S. J., & Yang, Q. (2010). A survey on transfer learning. *IEEE Transactions*
 424 *on Knowledge and Data Engineering*, 22(10), 1345–1359. doi: 10.1109/TKDE
 425 .2009.191
- 426 Perez, L., & Wang, J. (2017). The Effectiveness of Data Augmentation in Image
 427 Classification using Deep Learning.
- 428 Prechelt, L. (1998). Early stopping-but when? In *Neural networks: Tricks of the*
 429 *trade* (pp. 55–69). Springer.
- 430 Raissi, M., Perdikaris, P., & Karniadakis, G. E. (2019). Physics-informed neural
 431 networks: A deep learning framework for solving forward and inverse problems
 432 involving nonlinear partial differential equations. *Journal of Computational*
 433 *Physics*, 378(October), 686–707. Retrieved from [https://doi.org/10.1016/](https://doi.org/10.1016/j.jcp.2018.10.045)
 434 [j.jcp.2018.10.045](https://doi.org/10.1016/j.jcp.2018.10.045) doi: 10.1016/j.jcp.2018.10.045
- 435 Rawat, W., & Wang, Z. (2017, sep). Deep Convolutional Neural Networks for Image
 436 Classification: A Comprehensive Review. *Neural Computation*, 29(9), 2352–
 437 2449. Retrieved from <http://arxiv.org/abs/1803.01446>[https://direct](https://direct.mit.edu/neco/article/29/9/2352-2449/8292)
 438 [.mit.edu/neco/article/29/9/2352-2449/8292](https://direct.mit.edu/neco/article/29/9/2352-2449/8292) doi: 10.1162/neco.a.00990
- 439 Reback, J., Jbrockmendel, McKinney, W., den Bossche, J. V., Augspurger, T.,
 440 Cloud, P., ... Seabold, S. (2021). *pandas-dev/pandas: Pandas 1.3.4*. Zen-
 441 odo. Retrieved from <https://doi.org/10.5281/zenodo.5574486> doi:
 442 10.5281/zenodo.5574486
- 443 Schultz, M. G., Betancourt, C., Gong, B., Kleinert, F., Langguth, M., Leufen, L. H.,
 444 ... Stadler, S. (2021). Can deep learning beat numerical weather prediction?
 445 *Philosophical Transactions of the Royal Society A: Mathematical, Physical and*
 446 *Engineering Sciences*, 379(2194). doi: 10.1098/rsta.2020.0097
- 447 SHOM. (2015). *MNT Bathymétrie de façade Atlantique*. doi: [http://dx.doi.org/](http://dx.doi.org/10.17183/MNT_ATL100m_HOMONIM_WGS84)
 448 [10.17183/MNT_ATL100m_HOMONIM_WGS84](http://dx.doi.org/10.17183/MNT_ATL100m_HOMONIM_WGS84)

- 449 Shorten, C., & Khoshgoftaar, T. M. (2019). A survey on Image Data Augmentation
450 for Deep Learning. *Journal of Big Data*, 6(1). Retrieved from [https://doi](https://doi.org/10.1186/s40537-019-0197-0)
451 [.org/10.1186/s40537-019-0197-0](https://doi.org/10.1186/s40537-019-0197-0) doi: 10.1186/s40537-019-0197-0
- 452 Sonogashira, M., Shonai, M., & Iiyama, M. (2020). High-resolution bathymetry
453 by deep-learning-based image superresolution. *PLoS ONE*, 15(7), 1–19. Re-
454 trieved from <http://dx.doi.org/10.1371/journal.pone.0235487> doi: 10
455 [.1371/journal.pone.0235487](https://doi.org/10.1371/journal.pone.0235487)
- 456 Stengel, K., Glaws, A., Hettlinger, D., & King, R. N. (2020). Adversarial super-
457 resolution of climatological wind and solar data. *Proceedings of the National*
458 *Academy of Sciences of the United States of America*, 117(29), 16805–16815.
459 doi: 10.1073/pnas.1918964117
- 460 Su, H., Wang, A., Zhang, T., Qin, T., Du, X., & Yan, X.-H. (2021). Super-resolution
461 of subsurface temperature field from remote sensing observations based on
462 machine learning. *International Journal of Applied Earth Observation and*
463 *Geoinformation*, 102, 102440. Retrieved from [https://doi.org/10.1016/](https://doi.org/10.1016/j.jag.2021.102440)
464 [j.jag.2021.102440](https://doi.org/10.1016/j.jag.2021.102440) doi: 10.1016/j.jag.2021.102440
- 465 Tolman, H. L. (2009). User manual and system documentation of WAVEWATCH III
466 TM version 3.14. *Technical note, MMAB Contribution*, 276, 220.
- 467 Um, K., Brand, R., Yun, Fei, Holl, P., & Thuerey, N. (2020). Solver-in-the-Loop:
468 Learning from Differentiable Physics to Interact with Iterative PDE-Solvers.
469 *34th Conference on Neural Information Processing Systems*, 1(c), 1–37. Re-
470 trieved from <http://arxiv.org/abs/2007.00016>
- 471 Willard, J., Jia, X., Xu, S., Steinbach, M., & Kumar, V. (2020). Integrating Physics-
472 Based Modeling with Machine Learning: A Survey. , 1(1), 1–34. Retrieved
473 from <http://arxiv.org/abs/2003.04919>
- 474 Xie, Y., Franz, E., Chu, M., & Thuerey, N. (2018). tempoGAN: a temporally co-
475 herent, volumetric GAN for super-resolution fluid flow. *ACM Transactions on*
476 *Graphics*, 37(4), 1–15. Retrieved from [https://dl.acm.org/doi/10.1145/](https://dl.acm.org/doi/10.1145/3197517.3201304)
477 [3197517.3201304](https://dl.acm.org/doi/10.1145/3197517.3201304) doi: 10.1145/3197517.3201304